Genomics 105 (2015) 220–228

Contents lists available at ScienceDirect

Genomics

journal homepage: www.elsevier.com/locate/ygeno

Rescue of gene-expression changes in an induced mouse model of spinal muscular atrophy by an antisense oligonucleotide that promotes inclusion of *SMN2* exon 7

John F. Staropoli [a,1], Huo Li [a,1], Seung J. Chun [b], Norm Allaire [a], Patrick Cullen [b], Alice Thai [a], Christina M. Fleet [a], Yimin Hua [c], C. Frank Bennett [b], Adrian R. Krainer [c], Doug Kerr [a], Alexander McCampbell [a], Frank Rigo [b], John P. Carulli [a,*]

[a] Division of Genetics and Genomics, Biogen Idec, 12 Cambridge Center, Cambridge, MA 02142, USA
[b] Neuroscience Drug Discovery, Isis Pharmaceuticals, Inc., 2855 Gazelle Court, Carlsbad, CA 92010, USA
[c] Cold Spring Harbor Laboratory, 1 Bungtown Road, Cold Spring Harbor, NY 11724, USA

ARTICLE INFO

Article history:
Received 9 January 2015
Accepted 25 January 2015
Available online 31 January 2015

Keywords:
Spinal muscular atrophy
Gene expression
Mouse model
SMN2
Antisense
Oligonucleotide

ABSTRACT

Spinal muscular atrophy (SMA) is a neuromuscular disease caused by disruption of the *survival motor neuron 1* (*SMN1*) gene, partly compensated for by the paralogous gene *SMN2*. Exon 7 inclusion is critical for full-length SMN protein production and occurs at a much lower frequency for *SMN2* than for *SMN1*. Antisense oligonucleotide (ASO)-mediated blockade of an intron 7 splicing silencer was previously shown to promote inclusion of *SMN2* exon 7 in SMA mouse models and mediate phenotypic rescue. However, downstream molecular consequences of this ASO therapy have not been defined. Here we characterize the gene-expression changes that occur in an induced model of SMA and show substantial rescue of those changes in central nervous system tissue upon intracerebroventricular administration of an ASO that promotes inclusion of exon 7, with earlier administration promoting greater rescue. This study offers a robust reference set of preclinical pharmacodynamic gene expression effects for comparison of other investigational therapies for SMA.

1. Introduction

Spinal muscular atrophy (SMA) is an autosomal recessive neuromuscular disorder in which progressive α-motor neuron degeneration leads to weakness and atrophy of primarily proximal skeletal muscles [1]. The underlying genetic defect is the loss of function, usually deletion, of *survival motor neuron 1* (*SMN1*) [2], which encodes the protein SMN involved in the assembly of small nuclear ribonucleoprotein complexes [3]. A neighboring gene centromeric to *SMN1* at chromosome 5q13, *SMN2*, arose from duplication and subsequent mutation of *SMN1* and is unique to humans [4]. The handful of nucleotide differences between *SMN1* and *SMN2* include a C>T transition in *SMN2* at position 6 of exon 7. Together with an intronic splicing silencer (ISS) in intron 7, termed ISS-N1 [5], this nucleotide difference suppresses inclusion of exon 7, thereby encoding a truncated protein product, SMNΔ7, which is essentially non-functional and rapidly degraded. However, at some frequency, *SMN2* does generate transcripts that include exon 7 and encode a full-length SMN protein identical to that encoded by *SMN1*.

SMN2 is itself subject to gene duplication, and its copy number is the major genetic modifier of SMA phenotype from type I (severe with infantile onset) to type IV (mild with adult onset). This pattern is recapitulated in murine models of SMA in which knockout of the single murine *Smn* gene, which results in embryonic lethality [6], can be rescued by a variable copy number of the human *SMN2* transgene. *Smn* knockout mice with two copies of *SMN2* ($Smn^{-/-}$; $SMN2^{+/0}$) model a severe form of SMA, with mice surviving ~1 week [7,8]. A strain with an additional human *SMN2* complementary DNA (cDNA) transgene lacking exon 7 ($Smn^{-/-}$; $SMN2^{+/0}$; *SMNΔ7*) lives to ~15 days [9]. Mice with four copies of the *SMN2* transgene ($Smn^{-/-}$; $SMN2^{+/+}$) model a very mild form of SMA and have a normal lifespan, but develop ear and tail necrosis likely secondary to vascular deficits [7].

The partly compensatory activity of *SMN2* has made it an attractive target for molecules that promote inclusion of exon 7 and therefore increase the level of functional SMN protein in the setting of *SMN1*

Abbreviations: ASO, antisense oligonucleotide; *Cdkn1A*, cyclin-dependent kinase inhibitor 1A; cDNA, complementary DNA; FDR, false discovery rate; FUS, fused in sarcoma; *Hist1H1C*, histone cluster 1, H1C; ICV, intracerebroventricular; ISS, intronic splicing silencer; P, post-natal day; Partek GS, Partek® Genomics Suite™; PBS, phosphate-buffered saline; PCR, polymerase chain reaction; qPCR, quantitative polymerase chain reaction; RT, reverse transcription; SMA, spinal muscular atrophy; SMN, survival motor neuron; snRNP, small nuclear ribonucleoprotein.

* Corresponding author. Fax: +1 617 679 3200.
E-mail address: john.carulli@biogenidec.com (J.P. Carulli).

[1] These authors contributed equally.

http://dx.doi.org/10.1016/j.ygeno.2015.01.007

deficiency. Indeed, a 2′-*O*-(2-methoxyethyl)-modified antisense oligonucleotide (ASO), designated ASO 10-27, targets a site within intron 7 that overlaps with ISS-N1 and promotes efficient inclusion of *SMN2* exon 7. ASO 10-27, which mediates partial phenotypic rescue of both severe and mild models of SMA [10,11], also is known as ISIS-SMN_{Rx}, a drug currently undergoing investigation in children and infants with SMA.

In evaluating the pharmacodynamic profile and therapeutic efficacy of candidate compounds, a model with an intermediate phenotype is of particular value. Therefore, an induced model of SMA was developed by administering adult mice with mild SMA an ASO, designated ASO 20-37, that targets a purine-rich exon splicing enhancer region in the middle of exon 7 and promotes skipping of *SMN2* exon 7 beyond background levels of exon 7 exclusion [12,13]. We recently described the phenotypic and histopathologic effects of induced SMN depletion and repletion with ASO 20-37 (skip) and ASO 10-27 (therapeutic), respectively, delivered by intracerebroventricular (ICV) injection in neonatal [12] and adult [13] mice with SMA. The consequences of *SMN2* mis-splicing were progressive and dose dependent. For instance, in 2-month-old mice administered the skip ASO 20-37, effects on body weight and locomotor activity were apparent by day 30 after injection of the 100-μg dose, but not until after day 60 at the 25-μg dose. SMA-like pathology appeared in parallel and included reduced α-motor neuron density, neuromuscular junction defects, decreased muscle fiber sizes and reduced numbers of central synapses onto motor neurons. Early ICV, but not intraperitoneal, administration of the therapeutic ASO 10-27 at 5 or 22 days after ICV delivery of the skip ASO 20-37 significantly prolonged survival and reversed the subset of abnormal phenotypes analyzed.

In this report, we describe the gene-expression signature of the foregoing induction and rescue paradigm. Previous expression profiling of a severe model [14] was likely confounded by marked developmental changes that normally occur in the spinal cord of neonatal mice [15]. Moreover, expression changes secondary to profound tissue damage in models of severe SMA may mask dysregulation that is a direct consequence of SMN loss of function, although a recent study attempted to circumvent these potential effects by analyzing overtly pre-symptomatic post-natal day 1 (P1) mice [16]. We show that induction of SMA in adult mice did not yield significant gene-level expression changes until 30 days post-induction and that many of these changes could be prevented or reversed by administration of an ASO that promotes exon 7 inclusion, with earlier treatment improving survival and degree of transcriptional rescue. These data provide an important catalog of pharmacodynamic biomarkers of SMN depletion and restoration that can guide preclinical evaluation of novel SMA therapeutics. In addition, this analysis highlights molecular pathways proximal to SMN function, including cell-cycle signaling, for which recent evidence has emerged from independent analyses of SMN protein function and models of SMA.

2. Results

2.1. Physiologic early post-natal gene-expression changes in the mouse spinal cord far exceed genotype-driven changes in a model of severe SMA

We first sought to evaluate whether a well-characterized model of severe SMA could serve as a tool for pharmacodynamic monitoring on the basis of gene-expression. We used 3′ microarrays to assess gene-level expression in spinal cord tissue from mice with severe SMA ($Smn^{-/-}$; $SMN2^{+/0}$) [17,18]. Because these mice survive only ~10 days, analysis was necessarily limited to the early post-natal period; tissue was analyzed from five mice each at P1 and P5. Littermates heterozygous for endogenous *Smn* and carrying four copies of the human transgene ($Smn^{+/-}$; $SMN2^{+/+}$) [7] served as the comparator group (n = 5 for each time point). The vast majority of changes were driven by developmental stage (P1 versus P5) rather than by genotype (control versus SMA; Fig. 1 and Supplemental dataset S1), consistent with previous findings in the $Smn^{-/-}$; $SMN2^{+/0}$; *SMNΔ7* models at P1, P7 and P13 [15]. In fact, changes in the control group between P1 and P5 were even greater than those in the SMA group during the same period, suggesting that the developing spinal cord undergoes significant physiologic changes in the early post-natal period. Of note, among the few genotype-driven changes at P5, up-regulation of the transcripts for cyclin-dependent kinase inhibitor 1A (*Cdkn1a*; p21) and histone cluster 1, H1c (*Hist1H1C*) also had been reported as genotype-driven changes at P7 in the $Smn^{-/-}$, $SMN2^{+/0}$, *SMNΔ7* model [15].

2.2. Induction of SMA in adult mice causes a delayed and coordinated transcriptional response

Given that (1) few genotype-driven changes were present in a model of severe SMA and (2) significant early post-natal expression changes in the mouse spinal cord would likely confound any changes mediated by ASO therapy, we decided to analyze gene-expression changes in a more recently characterized induced model of SMA [12,13]. To evaluate the time course of transcriptional changes induced by skipping *SMN2* exon 7 beyond background levels of exon 7 exclusion, 15-week-old mice with mild SMA ($Smn^{-/-}$; $SMN2^{+/+}$) [7] were given a single ICV bolus injection of 50 μg exon 7 skip ASO 20-37 or a control ASO, and central nervous system tissue (spinal cord and brain) was collected 10, 20 or 30 days after treatment (Table 1). Median survival at this dose and age of administration was 37 days with the skip ASO (Fig. 2A), falling between the median survival of 70 and 34 days at the 25-μg and 100-μg doses, respectively, as reported in our previous study [13]. Reverse transcription (RT) polymerase chain reaction (PCR) for the *SMN2* transgene from the lumbar cord (Fig. 2B) and brain (Supplemental Fig. S1) showed that the skip ASO induced a progressive suppression of exon 7 inclusion between days 10 and 30 post injection. The control ASO had a minimal effect on *SMN2* splicing over the same interval in the lumbar cord and brain (Fig. 2B and Supplemental Fig. S1).

To identify global expression changes induced by acute SMN depletion, the cervical portions of the spinal cords from the above mice were used to analyze gene-level changes using 3′ arrays as well as exon-level changes using a microarray with 750,000 probes covering 250,000 exons. Unsupervised hierarchical clustering analysis of gene-level expression changes post injection showed stable expression patterns at days 10 and 20 post injection, but marked changes at day 30 across the cohort receiving the skip ASO (Figs. 2C and D and Supplemental Dataset S2). The only statistically significant gene-level changes that overlapped with genotype-driven changes in the severe model assessed above were up-regulation of the transcripts for *Cdkn1a* (p21) and *Hist1H1C* and down-regulation of the transcript for albumin D-box binding protein (*Adbp*). Two of these changes (up-regulation of *Cdkn1a* and *Hist1H1C*) overlapped with the set of genotype-driven changes observed at day 7 in the $Smn^{-/-}$; $SMN^{+/-}$; *SMNΔ7* models [15], suggesting that these are molecular signals closely linked to SMN function, robust across several models of SMA and independent laboratories. A more recent study using RNA-Seq of laser-capture-microdissected motor neurons from $Smn^{-/-}$; $SMN^{+/-}$; *SMNΔ7* mice at post-natal day 1 also showed significant upregulation of *Cdkn1a* [16]. Eleven other up-regulated transcripts were shared between these datasets (Supplemental Fig. S2) and included components of the C1q complex, whose upregulation is hypothesized to promote overpruning of synapses in the severe model of SMA [16]. Pathway analysis of altered transcripts in the current study showed a significant enrichment of gene ontology terms for the complement system, cell cycle signaling and apoptosis signaling (Table 2).

Statistically significant exon-level changes were relatively few and, as with the gene-level changes, appeared primarily at day 30 post-induction (Supplemental Table S1). A subset of exons whose expression was altered relative to constitutively expressed exons from the same gene was analyzed on a microfluidic quantitative PCR (qPCR) platform

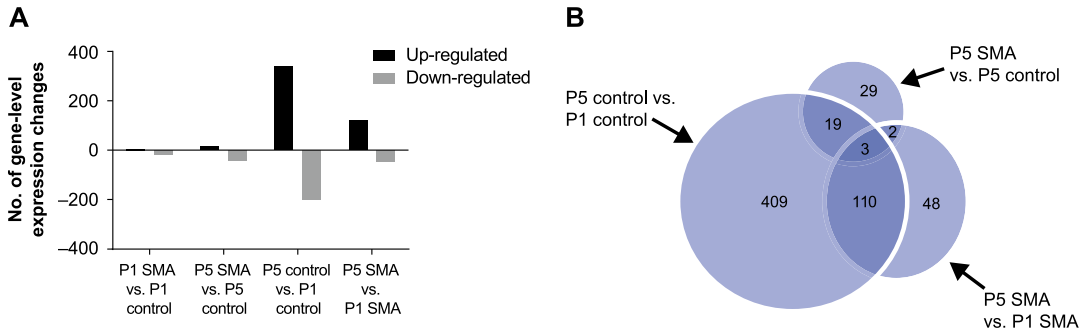

Fig. 1. (A) Gene-level expression changes in spinal cord tissue of an uninduced model of severe SMA (*Smn*$^{-/-}$; *SMN2*$^{+/0}$) versus control littermates (*Smn*$^{+/-}$; *SMN2*$^{+/+}$) at P1 and P5; n = 5 for each group. Fold changes ≥1.5 with an FDR-adjusted *P*-value < 0.05 are shown. (B) Venn diagram showing relationship between gene-expression changes presented in (A). The small number of changes in the P1 SMA versus P1 control comparison is omitted for clarity. FDR, false discovery rate; P, post-natal day; SMA, spinal muscular atrophy; SMN, survival motor neuron.

(Fluidigm Corporation), and the results were consistent with those obtained by microarray (Supplemental dataset S3 and text file S1).

2.3. Induced transcriptional changes can be prevented or reversed in a time-dependent manner with an ASO-promoting inclusion of SMN2 exon 7

Given that most transcriptional changes occurred 30 days post-induction, we sought to determine whether those changes could be prevented before that point or reversed at that point by administration of a 20-mer ASO that, similar to ISIS-SMN$_{Rx}$, blocks the intron 7 splicing silencer ISS-N1 and enhances inclusion of *SMN2* exon 7. Eight-week-old mice were treated with the skip or control ASO, and then with the therapeutic ASO on day 20, 25 or 30 after disease induction. The complete list of treatments is given in Table 3.

As in the 15-week-old cohort used in the first induction experiment, median survival was 37 days post-induction with no further treatment. When administered on day 20, the therapeutic ASO prevented death of all six mice in the cohort until at least day 54, but rescue was incomplete when administration of the therapeutic ASO was delayed to day 25 or 30 post-induction (Fig. 3A). The therapeutic ASO promoted inclusion of exon 7 in the *SMN2* transcript (Fig. 3B) and increased SMN protein levels as assessed by immunoblotting of spinal cord whole cell lysates (Fig. 3C) and immunohistochemistry of thoracic spinal cord sections (Fig. 3D). Mice injected with the skip or control ASO (groups D and E; Table 3) were sacrificed 30 days later and their spinal cords were removed for gene-expression profiling performed as described above to assess the reproducibility of day 30 expression changes obtained in the first induction experiment. The mice that received the therapeutic ASO on day 20, 25 or 30 post-induction and survived to day 54 (six of six, five of six, and three of six animals, respectively) were sacrificed at that point and analyzed similarly.

A total of 363 transcripts changed by ≥1.5-fold with the skip ASO versus control ASO treatment at day 30 (group D versus E; Table 3 and Supplemental dataset S4). Of these, 132 transcripts changed by ≥2-fold and these changes overlapped substantially with those in the first induction experiment in 15-week-old mice (Fig. 4A; hypergeometric *P*-value = 6.8×10^{-144}), supporting the robustness of our analysis. The second cohort (8 weeks old) was 7 weeks younger than the first cohort; therefore, the consistency of the data also suggested that most transcriptional changes indeed arose from induced SMN depletion, rather than physiologic post-developmental changes during this period of adulthood.

Table 1
SMA induction experiment.

Group no.	Injection D0	Day of sacrifice	No. of mice
A	PBS	10	5
B	Control ASO, 50 μg	10	5
C	Control ASO, 50 μg	20	5
D	Control ASO, 50 μg	30	5
E	Skip ASO, 50 μg	10	5
F	Skip ASO, 50 μg	20	5
G	Skip ASO, 50 μg	30	7

ASO, antisense oligonucleotide; D, day; PBS, phosphate-buffered saline; SMA, spinal muscular atrophy.

Administration of the therapeutic ASO at day 20 post-induction (group I; Table 3) prevented 248 of 363 (68%) transcripts from changing by >50% of their baseline (control ASO treated) levels at the time of analysis (day 54 post-induction; Figs. 4B and C and Supplemental dataset S4). The percentage of rescued transcripts at this same time point fell to 47% when administration of the therapeutic ASO was delayed to day 25 post-induction (group J); these transcripts were a complete subset of those rescued in group I. By day 30 post-induction, when most of the skip ASO-induced changes had set in, the therapeutic ASO restored 31% of altered transcripts to >50% of their baseline levels (group K); these were a complete subset of those rescued in group J, with the exception of one transcript (*Agxt2l1*), which appeared among the rescued transcripts in groups I and K but not those in group J. An example of a transcript for which the therapeutic ASO both prevented and reversed changes induced by the skip ASO is *Gdf15* (Fig. 4D, left panel). *Tgfbi* is an example of a transcript for which the change was prevented by the therapeutic ASO at day 20 or 25 post-induction, but not reversed when administration was delayed to day 30 post-induction (Fig. 4D, right panel). Pathway analysis of rescued transcripts revealed that cell cycle signaling was the most significantly represented pathway both among transcripts prevented from changing by therapeutic ASO administration at day 20 or 25 (Table 4) and among transcripts that had already changed and were reversed by therapeutic ASO administration at day 30 (Table 5).

Selected transcripts with statistically significant changes were analyzed on a microfluidic qPCR platform (Fluidigm Corporation), and fold changes were consistent with the microarray results (Supplemental dataset S5 and text file S2). Given recent reports of a functional association between SMN and genes implicated in amyotrophic lateral sclerosis [19,20], we also analyzed expression of the transcripts for fused in sarcoma (*Fus*), TAR DNA-binding protein (*Tardbp*) and valosin-containing protein (*Vcp*) in this analysis and confirmed the lack of significant expression changes observed by microarray (Supplemental dataset S5).

Selected transcripts that were significantly altered at day 30 post-induction, including *Sgca*, *Eda2r*, *Igfbp2*, *Cdkn1a*, *Tgfbi*, and *Ifi44*, were mostly unchanged at the protein level, as assessed by immunoblotting of corresponding spinal cord lysates (Supplemental Fig. S3 and data not shown). Of this group, only *Igfbp2* was significantly changed (~1.7-fold increase in skip versus therapeutic ASO-treated mice). This

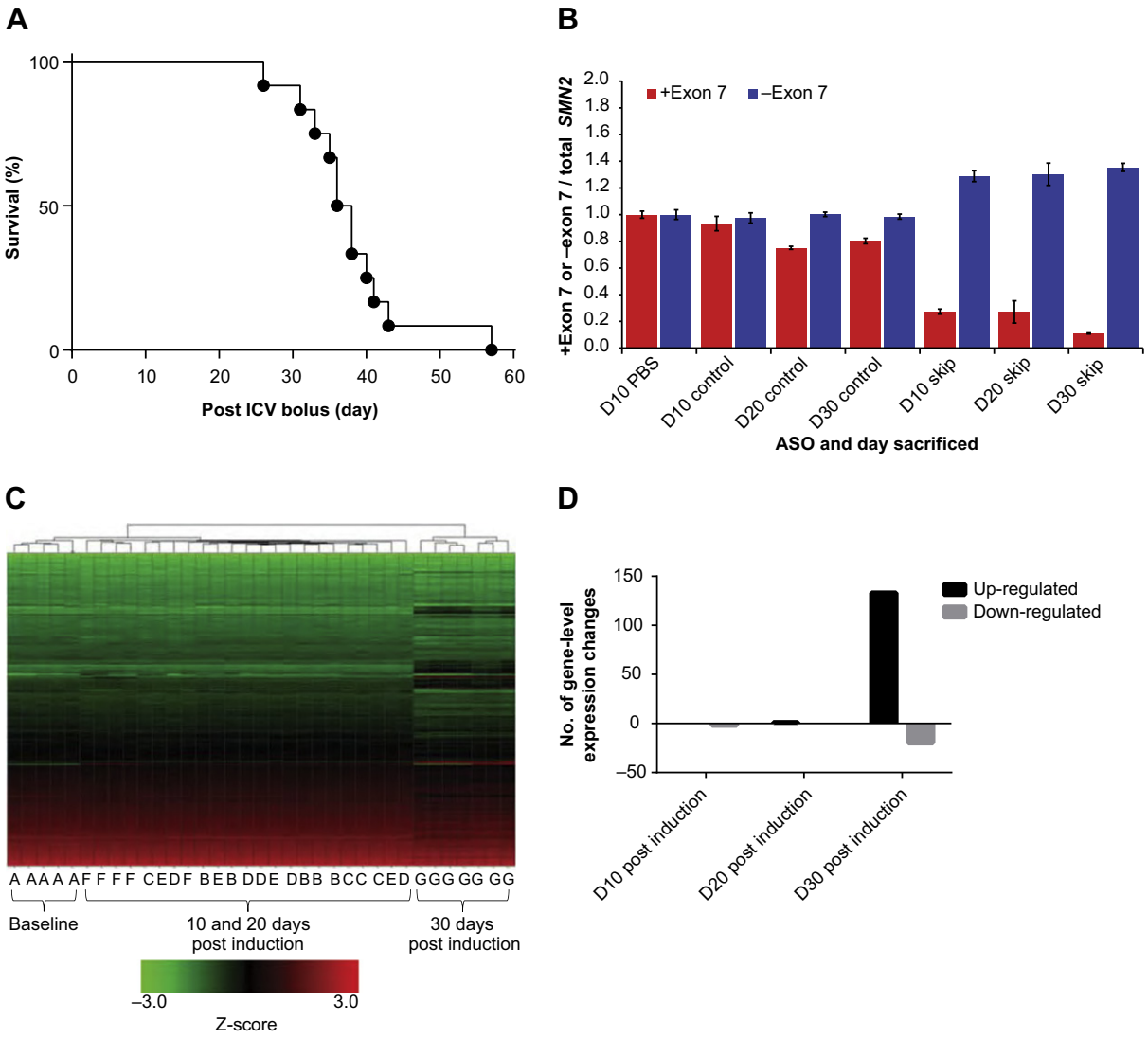

Fig. 2. (A) Kaplan–Meier survival curve of 15-week-old mice with mild SMA (*Smn*$^{-/-}$; *SMN2*$^{+/+}$; n = 12) given an ICV bolus injection of 50 μg skip ASO 20-37. (B) RT-PCR quantification of exon 7 inclusion or exclusion in the spinal cord as a fraction of total *SMN2* transcript for each of the cohorts described in Table 1. Data were normalized to the PBS-treated cohort (group A). (C) Unsupervised hierarchical clustering analysis of gene-level expression changes for the cohorts described in Table 1. Letters on the horizontal axis correspond to individual animals in each of the designated cohorts. The heat map shows a Z-score transformation of probe intensity values compared to the population mean. (D) Quantification of gene-expression changes induced by skip oligo at D10, D20 and D30 post induction in spinal cord tissue with ≥2-fold change and FDR <0.05. ASO, antisense oligonucleotide; D, day; FDR, false discovery rate; ICV, intracerebroventricular; PBS, phosphate-buffered saline; RT-PCR, reverse transcription polymerase chain reaction; SMA, spinal muscular atrophy; SMN, survival motor neuron.

Table 2
Pathway analysis of gene-expression changes induced by skip oligo at D30.

Ingenuity canonical pathways	−log(*P*)
Complement system	5.15
Cell cycle signaling	5.09
Apoptosis signaling	5.03
Fcγ receptor-mediated phagocytosis	4.82
Acute phase response signaling	4.46
Tissue remodeling	4.41
Dendritic cell maturation	4.34
NK cell signaling	3.02
Death receptor signaling	2.81
Crosstalk between dendritic and NK cells	2.79

Pathway analysis of gene-expression changes induced by skip oligo at D30. Top canonical pathways and Fisher's exact test-derived *P*-values for enrichment are shown.
D, day; NK, natural killer.

discordance between gene expression and protein changes has been observed in other models of SMN [21]. Notably, although gemin 2 and gemin 8 were not altered at the level of gene expression, the protein levels of both significantly increased with therapeutic ASO treatment, consistent with the observation that SMN stabilizes gemin proteins [3].

3. Discussion

In this study, we set out to characterize transcriptional changes most proximal to SMN function that therefore represent candidate biomarkers for therapeutic engagement by an ASO that increases levels of full-length SMN by promoting inclusion of exon 7 in the *SMN2* transcript. Selecting the proper model for this analysis among the many that have been characterized is of critical importance. Murine models of severe SMA highlight the critical role of SMN in early pre- and post-synaptic development of the neuromuscular junction [7,9,11], but the

Table 3
Treatment plan to evaluate prevention/reversal of induced transcriptional changes.

Group no.	Injection D0	Injection D20	Day of sacrifice	No. of mice
A	PBS	None	20	4
B	Skip ASO, 50 μg	None	20	4
C	Control ASO, 50 μg	None	20	4
D	Skip ASO, 50 μg	None	30	5
E	Control ASO, 50 μg	None	30	5
F	Skip ASO, 50 μg	Therapeutic ASO, 100 μg	40	6
G	Control ASO, 50 μg	Therapeutic ASO, 100 μg	40	6
H	Skip ASO, 50 μg	None	Survival curve	6
I	Skip ASO, 50 μg	Therapeutic ASO at D20, 100 μg	54	6[a]
J	Skip ASO, 50 μg	Therapeutic ASO at D25, 100 μg	54	6[b]
K	Skip ASO, 50 μg	Therapeutic ASO at D30, 100 μg	54	6[c]

ASO, antisense oligonucleotide; D, day; PBS, phosphate-buffered saline.
[a] All six mice survived at D54.
[b] Five of six mice survived at D54.
[c] Three of six mice survived at D54.

concomitant profound effect on overall post-natal development and survival makes it difficult to separate transcriptional responses primary to SMN function from those secondary to degenerative changes. Moreover, significant changes in the spinal cord transcriptome are associated with normal development in the early post-natal period [15]. Our own analysis reproduced the finding that transcriptional changes in the spinal cord in the first post-natal week far outnumber any genotype-driven changes during the same period. We therefore used an induced adult model of SMA to minimize the confounding effects of early post-natal development on the transcriptional signature of SMN deficiency.

The current study showed that the extent of molecular rescue was time dependent, with earlier administration of the therapeutic ASO

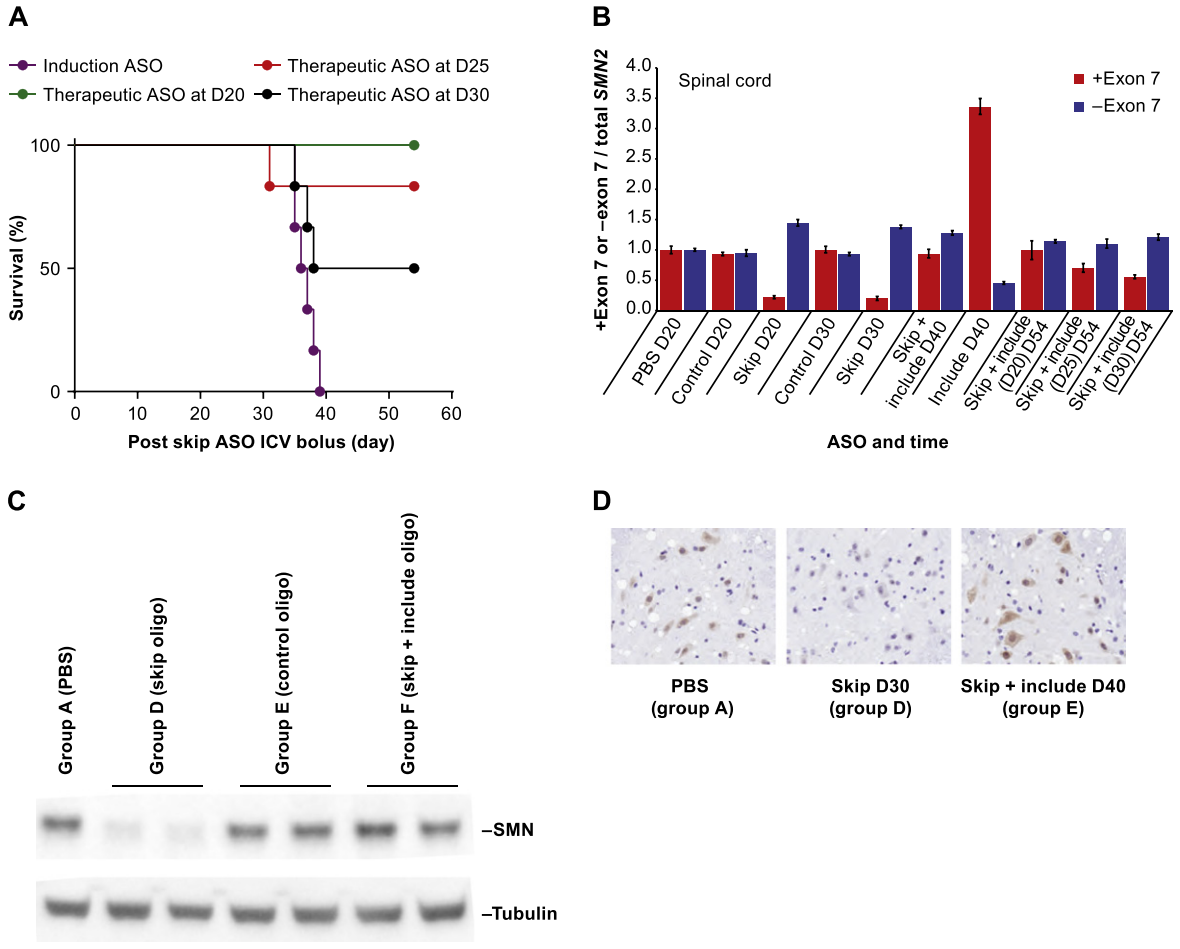

Fig. 3. (A) Kaplan–Meier survival curves for 8-week-old mice with mild SMA treated as described in Table 3. Curves are presented for groups H–K. All mice surviving to D54 were sacrificed for further analysis. (B) RT-PCR quantification of exon 7 inclusion or exclusion in the spinal cord as a fraction of total *SMN2* transcript for each of the cohorts described in Table 3. Data were normalized to the PBS-treated cohort (group A). (C) Immunoblotting of whole cell spinal cord lysates prepared from individual animals in the indicated treatment groups. The blot was probed first for SMN and then re-probed for α-tubulin. (D) Representative anti-SMN immunohistochemistry of thoracic spinal cord sections from the indicated treatment groups. ASO, antisense oligonucleotide; D, day; ICV, intracerebroventricular; PBS, phosphate-buffered saline; RT-PCR, reverse transcription polymerase chain reaction; SMA, spinal muscular atrophy; SMN, survival motor neuron.

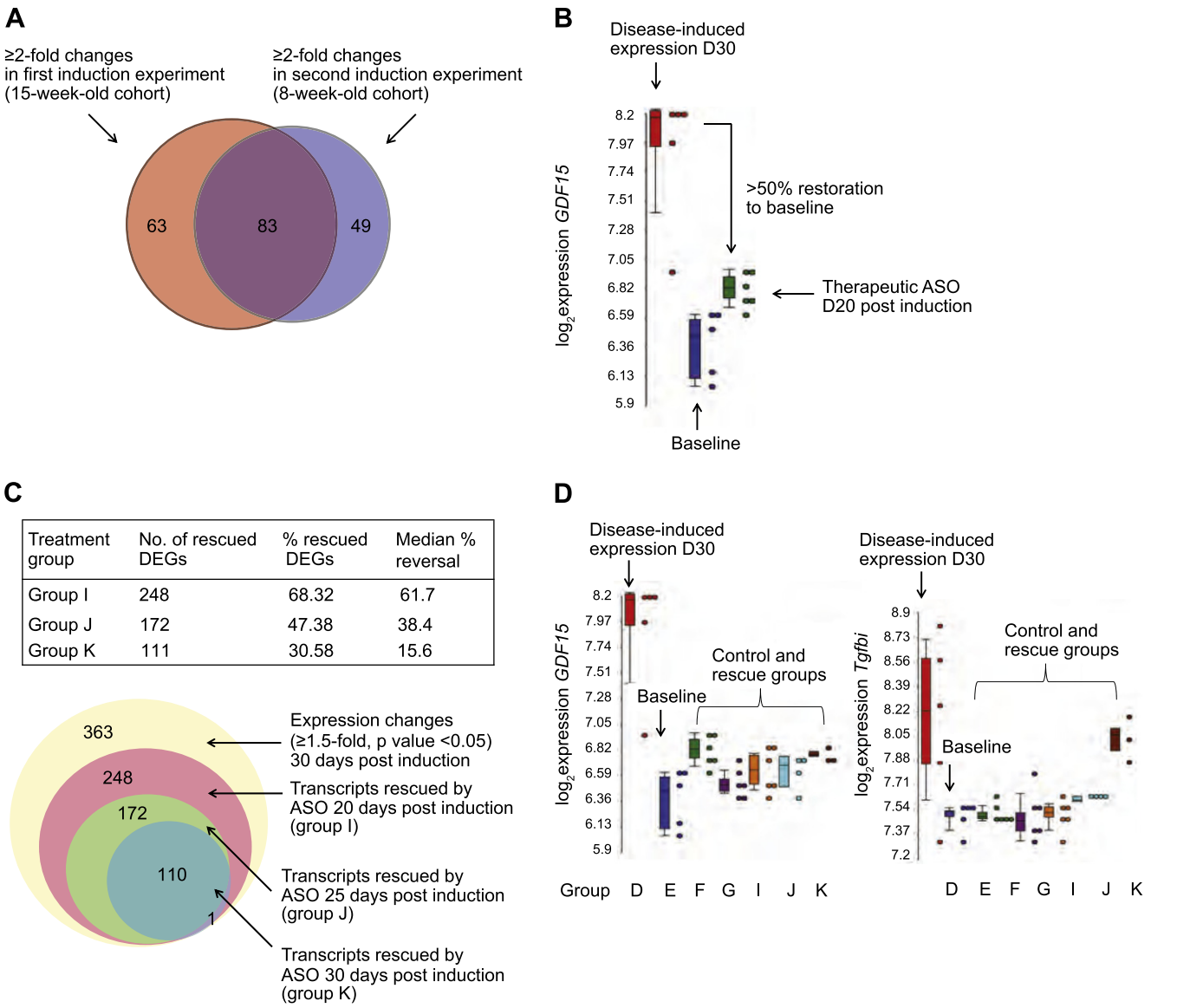

Treatment group	No. of rescued DEGs	% rescued DEGs	Median % reversal
Group I	248	68.32	61.7
Group J	172	47.38	38.4
Group K	111	30.58	15.6

Fig. 4. (A) Overlap of gene-level expression changes (≥2-fold; FDR <0.05) induced by ASO 20-37 at D30 in the first cohort (group G versus group D; Table 1) versus the second cohort (group D versus group E; Table 3). The probability that this subset of genes overlapped by chance, $P = 6.82 \times 10^{-144}$, is based on the hypergeometric distribution and the observation that ≥15 000 unique genes were detectable in mouse spinal cord by the microarray platform used in this study. (B) Rescued transcripts are defined as those whose expression levels are restored to ≥50% of their baseline (control ASO treated) levels. (C) Number of DEGs induced by ASO 20-37 at D30 (363 total DEGs with ≥1.5-fold changes; FDR <0.05) that are rescued in the indicated treatment group (groups I, J and K; Table 3). Median percentage reversal indicates the median degree of reversal to baseline expression across all 363 DEGs. The Venn diagram shows the relationship between rescued transcripts for groups I, J and K. (D) (Left) Rescue of *Gdf15* expression level with therapeutic ASO at D20 (group I), D25 (group J) and D30 (group K) post induction. (Right) Rescue of *Tgfbi* expression level with therapeutic ASO at D20 (group I) and D25 (group J) but not at D30 (group K) post induction. Each dot represents data from an individual animal, and box-and-whisker plots show median, first and third quartiles and outlier-excluded ranges for expression data in a given treatment group. ASO, antisense oligonucleotide; D, day; DEG, differentially expressed gene; FDR, false discovery rate.

(i.e. day 20 post-induction) showing better resolution of the expression profile than later administration (i.e. day 25 or 30 post-induction). Consistent with a previous report that exon-level changes are a late occurrence in SMN-deficient mice and more likely reflect secondary rather than primary effects of SMN deficiency on splicing [15], we identified few differential splicing signals upon ASO-induced SMN depletion. This reproducible finding was somewhat surprising, given the defined role of SMN in spliceosomal small nuclear ribonucleoprotein (snRNP) biogenesis [3,14], suggesting that splicing is relatively robust to the altered snRNP repertoire in the setting of SMN deficiency and raising the possibility of an incompletely elucidated compensatory pathway. Of note, a recent RNA-Seq analysis of laser capture-microdissected motor neurons from P1 *Smn*$^{-/-}$; *SMN2*$^{+/0}$; *SMNΔ7* mice revealed ~100 splicing aberrations, mostly in genes whose overall expression was unchanged [16]. This remains a small number of splicing changes given the purported centrality of SMN in snRNP biogenesis.

In the current study, SMN depletion had a far greater effect on gene-level expression than on detectable splicing events. Interestingly, gene ontology pathway analysis of transcripts most robustly rescued by the therapeutic ASO revealed that cell cycle signaling pathways were the most significantly represented. This finding is consistent with independent lines of evidence that have demonstrated an impact of SMN deficiency on DNA replication and possibly DNA repair, and have suggested that SMA is not only a degenerative disorder, but also a neurodevelopmental disorder. Developing *Drosophila* larvae showed a temporospatial gradient of Smn protein, with levels in the central nervous system highest in proliferative post-embryonic neuroblasts [22]. Loss or gain of *Smn* function disrupts larval growth and germline stem cell proliferation and

Table 4
Top gene pathways prevented from changing in the induced model by administration of the therapeutic ASO.

Ingenuity canonical pathways	$-\log(P)$
Cell cycle signaling	8.89
Aryl hydrocarbon receptor signaling	5.22
Tec kinase signaling	2.97
Role of pattern recognition receptors	2.88
Cholecystokinin/gastrin-mediated signaling	2.80
Granulocyte adhesion and diapedesis	2.76
NRF2-mediated oxidative stress response	2.70
Agranulocyte adhesion and diapedesis	2.65
IL-8 signaling	2.63
PI3K/AKT signaling	2.49
Cell cycle: G1/S checkpoint regulation	2.37
IL-10 signaling	2.33
CCR5 signaling in macrophages	2.30
Glioblastoma multiforme signaling	2.21
Estrogen-mediated S-phase entry	2.21
VDR/RXR activation	2.17
Altered T cell and B cell signaling	2.05
Acute phase response signaling	2.00
Complement system	1.94
Glioma signaling	1.93
Oncostatin M signaling	1.91
IGF-1 signaling	1.91
Cell cycle regulation by BTG family proteins	1.89
IL-17A signaling in fibroblasts	1.89
HGF signaling	1.87

ASO, antisense oligonucleotide; CCR5, C-C chemokine receptor type 5; HGF, hepatocyte growth factor; IGF, insulin-like growth factor; IL, interleukin; VDR, vitamin D receptor; RXR, retinoid X receptor.

differentiation. Furthermore, a mouse model of severe SMA showed a significant reduction in brain weight and cell number, particularly in the hippocampus, secondary to reduced proliferative capacity, not increased apoptotic cell death [23].

These findings were not so surprising, given that nuclear Cajal bodies, spliceosome biogenesis factories of which SMN is a component, may have a role in the G1/S phase transition in proliferating Schwann cells [24]. SMN co-localizes with cyclin-dependent kinase 2 during this transition and also promotes assembly of the U7 snRNP, required for histone mRNA 3′ end processing [25]. Together, these findings suggest that SMN contributes to the coupling of DNA replication with histone gene transcription. Indeed, subsets of Cajal bodies had previously been found to physically associate with histone gene clusters on chromosomes 1 and 6 [26], one component of which, *Hist1H1C*, was among the earliest transcripts we found to be dysregulated in the induced SMA model. Our data also showed robust activation of transcripts associated with p53-mediated cell cycle arrest, including *Cdkn1a* (p21), *Ccng1* (cyclin G1), and *Gtse1* (G2 and S phase-expressed protein 1), suggesting that some form of DNA damage is proximal to SMN depletion. Evidence for perinatal DNA damage in a mouse model of severe SMA is consistent with this possibility [27].

SMN itself is recruited, through its N-terminal Tudor domain, to dimethylated histone H3K79 in the setting of the interphase centromere damage response [28]. Whether SMN is involved in executing this response or other forms of DNA repair, such as double-strand break repair, known to be mediated by another Tudor-domain protein, 53BP1, in an H3K79me-dependent manner [29], is a question that warrants further investigation. Of note, SMN has been shown to interact physically and functionally with FUS [20], an RNA- and DNA-binding protein that mediates double-strand break repair through a histone deacetylase-1-dependent mechanism [30]. SMN–gemin complexes and FUS associate within gems, nuclear depots of snRNPs that serve as markers of SMN abundance, and SMN overexpression overcomes the gem deficit of FUS mutant lines from patients with amyotrophic lateral sclerosis [20]. Whether gems or the closely associated Cajal bodies couple their roles in splicing and transcription with the DNA damage response is unknown. Although we cannot rule out the contribution of reactive glial proliferation to cell cycle expression changes in the SMA model, a recent study showed that purified motor neuron precursors derived from mouse SMA embryonic stem cells (ESCs) also show marked up-regulation of cell proliferation genes or proteins, including p21, encoded by *Cdkn1a* [21]. Curiously, p21 levels are up-regulated over 40-fold in SMA mESCs compared to control mESCs, whereas *Cdkn1a* mRNA levels are *down*-regulated 0.76-fold [21]. Together, these data suggest that post-transcriptional and post-translational regulation of certain mRNAs and proteins disrupted in SMA may depend on the cell cycle status of the cells studied (e.g. proliferating mESC-derived motor neuron precursors versus post-mitotic motor neurons of the spinal cord).

Determining definitively whether the global expression changes observed in this study are primary or secondary to SMN status will require further investigation, but our data clearly support the utility of induced models of severe disease, whereby the proximal consequences of gene depletion can be more cleanly dissociated from the more distal effects of tissue pathology. Together with post-induction rescue, this study highlights potential biomarkers and pathways of SMA progression and therapeutic response. As clinical trials for SMA progress, it will be important to assess whether these expression changes are translatable to the human disease and extend to other tissues or biofluids more accessible than spinal cord.

Table 5
Top gene pathways reversed in the induced model by administration of the therapeutic ASO.

Ingenuity canonical pathways	$-\log(P)$
Cell cycle signaling	6.19
Granulocyte adhesion and diapedesis	3.59
Inhibition of angiogenesis by TSP1	3.17
Interferon signaling	3.17
Cell cycle: G2/M DNA damage checkpoint regulation	2.84
Role of pattern recognition receptors in recognition of bacteria and viruses	2.84
Pancreatic adenocarcinoma signaling	2.67
Agranulocyte adhesion and diapedesis	2.60
PI3K/AKT signaling	2.45
Activation of IRF by cytosolic pattern recognition receptors	2.40
Cell cycle: G1/S checkpoint regulation	2.34
Hepatic fibrosis/hepatic stellate cell activation	2.26
Molecular mechanisms of cancer	2.10
Role of p14/p19ARF in tumor suppression	2.00
Proline degradation	2.00
Chronic myeloid leukemia signaling	1.92
Thyroid cancer signaling	1.76
Melanoma signaling	1.72
Role of RIG-1-like receptors in antiviral innate immunity	1.68

ASO, antisense oligonucleotide; IRF, interferon regulatory factor; TSP-1, thrombospondin-1.

4. Material and methods

4.1. Oligonucleotides

Synthesis and purification of all chemically modified oligonucleotides were performed as previously described [31]. Therapeutic ASO, 5′-ATTCACTTTCATAATGCTGG-3′; skip ASO, 5′-GTGAGCACCTTCCTTC TT-3′; and control ASO, 5′-CTCAGTAACATTGACACCAC-3′. ASOs are uniformly modified with 2′-*O*-methoxyethyl nucleotides and have a phosphorothioate backbone.

4.2. Dosing of mice

All protocols met ethical standards for animal experimentation and were approved by the Institutional Animal Care and Use Committee. Adult male and female mice with type III SMA (*Smn*$^{-/-}$; *SMN2*$^{+/+}$) were obtained from the Jackson Laboratory (FVB.Cg-Tg(*SMN2*)2Hung *Smn1*^{tm1Hung}/J, stock number 005058). The lyophilized ASOs were dissolved in sterile phosphate-buffered saline (PBS) without calcium or

magnesium and quantified by ultraviolet spectrometry. The ASOs were then diluted to the desired concentration required for dosing mice and sterilized through a 0.2 μm filter. ICV bolus injections were performed as previously described [13].

4.3. RT-PCR for SMN2 analysis

For the spinal cord, a 2 mm lumbar section was collected. For the brain, a 1 mm coronal section, 2 mm posterior to the injection site, was collected. Each piece of tissue was homogenized in a 2 ml tube containing Lysing Matrix D (MP Biomedicals, LLC), 500 μl Buffer RLT (QIAGEN) and 1% volume to volume ratio β-mercaptoethanol. Homogenization was performed for 20 s at 6000 rpm using a FastPrep Automated Homogenizer (MP Biomedicals, LLC). Lysate (10 μl) was used to isolate RNA with an RNeasy 96 Kit (QIAGEN) that included in-column DNA digestion with 50 U of DNase I (Invitrogen™). Real-time RT-PCR was performed as previously described [32], except that full-length *SMN2* transcripts were analyzed with primers 5′-GCTGATGCTTTGGG AAGTATGTTA-3′ and 5′-TTTGATTTTGTCTAAAACCCATATA-3′ and probe 5′FAM/TACATGAGTGGCTATCATACT/3′MGBNFQ. The full-length or Δ7 *SMN2* expression level was normalized to that of total *SMN2*, and this was further normalized to the level in PBS-treated mice.

4.4. Immunostaining and immunoblotting

Staining of SMN protein in mouse tissues was performed as previously described [10]. Protein from spinal cord tissue was extracted with RIPA buffer with protease and phosphatase inhibitors, run on 4%–12% Bis-Tris gels (Novex), and probed with the following antibodies: anti-SMN (BD 6106-46, 1:1000); anti-Gemin 2 (Abcam ab6084[2E17]; 1:500); anti-Gemin 8 (Santa Cruz 130669; 1:500); anti-Igfbp2 (R&D Systems AF797 0.2 μg/ml); anti-Eda2r (Abnova H0060401-D01P, 1:500); anti-Sgca (Origene TA314526, 1:1000); and anti-p21 (Cell Signaling cs2947, 1:1000).

4.5. Microarray profiling

4.5.1. RNA preparation

Snap-frozen mouse spinal cord or brain tissue was homogenized in QIAzol Lysis Reagent (QIAGEN) and processed to RNA according to the manufacturer's recommendation. Purified RNA was further cleaned using the RNeasy Mini Kit (QIAGEN) with on-column DNase treatment as specified by the manufacturer. RNA integrity was assessed using LabChip GX (PerkinElmer, Inc.); quantities and 260/280 ratios were assessed using DropSense96 (PerkinElmer, Inc.). RNA samples with an RNA quality score >7.5 were considered high quality and were used for downstream genomic applications.

4.5.2. Sample preparation for exon and 3′ arrays

Samples were prepared for exon arrays using 100 ng of total RNA. RNA was manually amplified and the resulting sense cDNA was fragmented and labeled using the using Ambion® WT Expression Kit for high-throughput robotics (Life Technologies Corporation) according to the manufacturer's recommendations. For 3′ arrays, automated sample amplifications and biotin labelings were carried out using 50 ng of total RNA with the Ovation RNA Amplification System V2, Ovation® Whole Blood Solution and Encore® Biotin Module (NuGEN Technologies, Inc.) according to the manufacturer's recommendations using a Biomek Fx^P automated liquid handler (Beckman Coulter).

4.5.3. Hybridization, washing, scanning and image generation

Ambion or NuGEN fragmented and labeled cDNA was hybridized overnight to GeneChip® Mouse Gene 1.1 ST or GeneChip® HT MG-430PM plate arrays for exon array analysis or 3′ analysis, respectively (Affymetrix, Inc.). Plate arrays were washed and stained on a GeneChip® Array Station automated liquid handler (Caliper Life Sciences) according to the manufacturer's recommendations. Plate arrays were then scanned and array images (.dat files) were generated using a GeneTitan® HT plate scanner (Affymetrix, Inc.). Probe cell intensity (.cel) and global quality metric (.rpt) files for each scanned image were generated and imported into Spotfire (TIBCO Spotfire) for visualization and comparison with the historical data from the same type of arrays.

4.5.4. Data analysis

Gene-expression analysis for the 3′ array was performed using R/Bioconductor (R version 2.11.1; Bioconductor), while exon arrays were analyzed using Partek® Genomics Suite™ (Partek GS; version 6.5; Partek Inc.). Probe sets mapped to the same transcript cluster were grouped together, and Guanine Cytosine Robust Multi-Array Analysis method was used for normalization. Differential gene-expression was measured by empirical Bayes *t*-statistics and *P*-values were adjusted for false discovery rate (FDR) correction. Selected genes with (1) a FDR-adjusted *P*-value ≤ 0.05 using the Benjamini–Hochberg multiple testing procedure [33] and (2) an absolute fold change difference between groups ≥ 1.5-fold were analyzed for high-throughput qPCR validation as described below.

The quality assurance, data normalization, principal component analysis, multiple dimensional scaling and reduction, box plots, dot plots and volcano plots for exon arrays were performed by Partek GS. Genes with alternative splicing were analyzed using the Partek GS mixed analysis of variance model. Errors from multiple exons within the same transcript cluster were assumed to be independent. Such conditional independence allows one to derive a joint multivariate normal distribution so that relevant parameters and their standard errors can be estimated. We invoked the ALT-SPLICE ANOVA option under the STAT menu per the Partek GS manual. *P*-values and *F*-statistics on the exon and group interactions were extracted from Partek GS outputs.

4.6. High-throughput qPCR validation

4.6.1. Primer probe design

TaqMan® MGB probes and primer sets were designed to exon junctions or within single exons using Primer Express® Software Version 3.0 (Life Technologies Corporation) using default settings.

4.6.2. cDNA synthesis, sample and assay preparation

RNA (200 ng) was treated with DNAse using DNase I, Amplification Grade (Invitrogen™) and reverse transcribed using the HighCapacity cDNA Reverse Transcription Kit (Life Technologies Corporation) according to the manufacturer's recommendations. The reverse transcribed cDNA was pre-amplified with pooled assays and the TaqMan® PreAmp Master Mix (2×; Life Technologies Corporation) according to the manufacturer's recommendations. Pre-amplified cDNA samples were prepared for loading into a 96 × 96 array by diluting 5-fold and mixing with 2× TaqMan® Gene Expression Master Mix (Life Technologies Corporation) and 20× gene-expression sample loading reagent. TaqMan 20× assays were pooled and mixed with 2× assay loading reagent to a final concentration of primers 9 μM and probe 2 μM in the 10× assay mix.

4.6.3. Array priming, loading, thermocycling and data collection

Dynamic arrays (96 × 96) from Fluidigm Corporation were primed using the Prime (136×) script in an integrated fluidic circuit controller HX according to the manufacturer's recommendations. Aliquots of 5 μL of 10× assay mix or prepared cDNA samples were added into a 96 × 96 dynamic array and loaded into the chip using the Load Mix (136×) script in an integrated fluidic circuit controller HX according to the manufacturer's recommendations. The loaded 96 × 96 arrays were then thermal mixed: 50 °C, 120 s; 70 °C, 1800 s; 25 °C, 600 s; followed by UNG and Hot Start: 50 °C, 120 s and 95 °C, 600 s; and thermocycled: 95 °C, 15 s; 60 °C, 60 s, for 40 cycles on the BioMark™

system (Fluidigm Corporation). Raw data were processed using linear derivative for baseline correction, quality threshold set to 0.65 and automatic Ct thresholds.

4.6.4. Analysis

Fluidigm data were quality controlled and normalized based on the expression levels of the housekeeping genes. After filtering out the quality control failures, data were normalized using the ΔΔ method [34]. The Ct values of the samples of interest were compared with universal human control values as the calibrator. The Ct values of both the calibrator and the samples of interest were normalized to an appropriate endogenous housekeeping gene. The normalized ΔΔ Ct values were analyzed in JMP 9.0.3 (SAS Institute Inc.) to evaluate any significant changes (FDR-adjusted P-value < 0.05) in gene expression.

4.7. Gene ontology and pathway analysis

Transcripts/genes from the above differential analysis were subjected to the enrichment test for gene ontology and pathway analysis using the Ingenuity Pathway Analysis tool (QIAGEN). Lists of the most enriched pathways and their P-values based on Fisher's exact test are presented.

Supplementary data to this article can be found online at http://dx.doi.org/10.1016/j.ygeno.2015.01.007.

Conflict of interest

S.J.C., C.F.B., and F.R. are employees of Isis Pharmaceuticals, Inc. J.F.S., H.L., N.A., P.C., A.T., C.M.F., D.K., A.M., and J.P.C. are employees of Biogen Idec. A.R.K. is a consultant to Isis Pharmaceuticals, Inc. Y.H. has no conflicts to report.

Acknowledgments

This work was supported in part by the St. Giles Foundation and the SMA Foundation (A.R.K.), neither of whom were involved in the preparation of this manuscript or the decision to submit the article for publication. Biogen Idec and Isis Pharmaceuticals provided funding for the acquisition, analysis, and interpretation of data and jointly decided to submit the manuscript for publication. Biogen Idec provided funding for editorial support in the development of this paper. Kristen DeYoung of Excel Scientific Solutions (Southport, CT, USA) copyedited and styled the manuscript per journal requirements. Biogen Idec reviewed and provided feedback on the paper to the authors. The authors had full editorial control of the paper, and provided their final approval of all content.

References

[1] S.T. Iannaccone, Spinal muscular atrophy, Semin. Neurol. 18 (1998) 19–26.
[2] S. Lefebvre, L. Bürglen, S. Reboullet, O. Clermont, P. Burlet, L. Viollet, B. Benichou, C. Cruaud, P. Millasseau, M. Zeviani, D. Le Paslier, J. Frézal, D. Cohen, J. Weissenbach, A. Munnich, J. Melki, Identification and characterization of a spinal muscular atrophy-determining gene, Cell 80 (1995) 155–165.
[3] D.J. Battle, M. Kasim, J. Yong, F. Lotti, C.K. Lau, J. Mouaikel, Z. Zhang, K. Han, L. Wan, G. Dreyfuss, The SMN complex: an assembly machine for RNPs, Cold Spring Harb. Symp. Quant. Biol. 71 (2006) 313–320.
[4] C.F. Rochette, N. Gilbert, L.R. Simard, *SMN* gene duplication and the emergence of the *SMN2* gene occurred in distinct hominids: *SMN2* is unique to *Homo sapiens*, Hum. Genet. 108 (2001) 255–266.
[5] N.K. Singh, N.N. Singh, E.J. Androphy, R.N. Singh, Splicing of a critical exon of human *Survival Motor Neuron* is regulated by a unique silencer element located in the last intron, Mol. Cell. Biol. 26 (2006) 1333–1346.
[6] B. Schrank, R. Götz, J.M. Gunnersen, J.M. Ure, K.V. Toyka, A.G. Smith, M. Sendtner, Inactivation of the survival motor neuron gene, a candidate gene for human spinal muscular atrophy, leads to massive cell death in early mouse embryos, Proc. Natl. Acad. Sci. U. S. A. 94 (1997) 9920–9925.
[7] H.M. Hsieh-Li, J.-G. Chang, Y.-J. Jong, M.-H. Wu, N.M. Wang, C.H. Tsai, H. Li, A mouse model for spinal muscular atrophy, Nat. Genet. 24 (2000) 66–70.
[8] U.R. Monani, M. Sendtner, D.D. Coovert, D.W. Parsons, C. Andreassi, T.T. Le, S. Jablonka, B. Schrank, W. Rossoll, T.W. Prior, G.E. Morris, A.H.M. Burghes, The human centromeric survival motor neuron gene (*SMN2*) rescues embryonic lethality in *Smn*$^{-/-}$ mice and results in a mouse with spinal muscular atrophy, Hum. Mol. Genet. 9 (2000) 333–339.
[9] T.T. Le, L.T. Pham, M.E.R. Butchbach, H.L. Zhang, U.R. Monani, D.D. Coovert, T.O. Gavrilina, L. Xing, G.J. Bassell, A.H.M. Burghes, SMNΔ7, the major product of the centromeric survival motor neuron (*SMN2*) gene, extends survival in mice with spinal muscular atrophy and associates with full-length SMN, Hum. Mol. Genet. 14 (2005) 845–857.
[10] Y. Hua, K. Sahashi, G. Hung, F. Rigo, M.A. Passini, C.F. Bennett, A.R. Krainer, Antisense correction of *SMN2* splicing in the CNS rescues necrosis in a type III SMA mouse model, Genes Dev. 24 (2010) 1634–1644.
[11] M.A. Passini, J. Bu, A.M. Richards, C. Kinnecom, S.P. Sardi, L.M. Stanek, Y. Hua, F. Rigo, J. Matson, G. Hung, E.M. Kaye, L.S. Shihabuddin, A.R. Krainer, C.F. Bennett, S.H. Cheng, Antisense oligonucleotides delivered to the mouse CNS ameliorate symptoms of severe spinal muscular atrophy, Sci. Transl. Med. 3 (2011) 72ra18.
[12] K. Sahashi, Y. Hua, K.K.Y. Ling, G. Hung, F. Rigo, G. Horev, M. Katsuno, G. Sobue, C.-P. Ko, C.F. Bennett, A.R. Krainer, TSUNAMI: an antisense method to phenocopy splicing-associated diseases in animals, Genes Dev. 26 (2012) 1874–1884.
[13] K. Sahashi, K.K.Y. Ling, Y. Hua, J.E. Wilkinson, T. Nomakuchi, F. Rigo, G. Hung, D. Xu, Y.-P. Jiang, R.Z. Lin, C.-P. Ko, C.F. Bennett, A.R. Krainer, Pathological impact of *SMN2* mis-splicing in adult SMA mice, EMBO Mol. Med. 5 (2013) 1586–1601.
[14] Z. Zhang, F. Lotti, K. Dittmar, I. Younis, L. Wan, M. Kasim, G. Dreyfuss, SMN deficiency causes tissue-specific perturbations in the repertoire of snRNAs and widespread defects in splicing, Cell 133 (2008) 585–600.
[15] D. Bäumer, S. Lee, G. Nicholson, J.L. Davies, N.J. Parkinson, L.M. Murray, T.H. Gillingwater, O. Ansorge, K.E. Davies, K. Talbot, Alternative splicing events are a late feature of pathology in a mouse model of spinal muscular atrophy, PLoS Genet. 5 (2009) e1000773.
[16] Z. Zhang, A.M. Pinto, L. Wan, W. Wang, M.G. Berg, I. Oliva, L.N. Singh, C. Dengler, Z. Wei, G. Dreyfuss, Dysregulation of synaptogenesis genes antecedes motor neuron pathology in spinal muscular atrophy, Proc. Natl. Acad. Sci. U. S. A. 110 (2013) 19348–19353.
[17] R.G. Gogliotti, S.M. Hammond, C. Lutz, C.J. Didonato, Molecular and phenotypic reassessment of an infrequently used mouse model for spinal muscular atrophy, Biochem. Biophys. Res. Commun. 391 (2010) 517–522.
[18] M. Riessland, B. Ackermann, A. Förster, M. Jakubik, J. Hauke, L. Garbes, I. Fritzsche, Y. Mende, I. Blumcke, E. Hahnen, B. Wirth, SAHA ameliorates the SMA phenotype in two mouse models for spinal muscular atrophy, Hum. Mol. Genet. 19 (2010) 1492–1506.
[19] T. Achsel, S. Barabino, M. Cozzolino, M.T. Carri, The intriguing case of motor neuron disease: ALS and SMA come closer, Biochem. Soc. Trans. 41 (2013) 1593–1597.
[20] T. Yamazaki, S. Chen, Y. Yu, B. Yan, T.C. Haertlein, M.A. Carrasco, J.C. Tapia, B. Zhai, R. Das, M. Lalancette-Hebert, A. Sharma, S. Chandran, G. Sullivan, A.L. Nishimura, C.E. Shaw, S.P. Gygi, N.A. Shneider, T. Maniatis, R. Reed, FUS-SMN protein interactions link the motor neuron diseases ALS and SMA, Cell Rep. 2 (2012) 799–806.
[21] M. Maeda, A.W. Harris, B.F. Kingham, C.J. Lumpkin, L.M. Opdenaker, S.M. McCahan, W. Wang, M.E. Butchbach, Transcriptome profiling of spinal muscular atrophy motor neurons derived from mouse embryonic stem cells, PLoS One 9 (2014) e106818.
[22] S.J. Grice, J.L. Liu, Survival motor neuron protein regulates stem cell division, proliferation, and differentiation in *Drosophila*, PLoS Genet. 7 (2011) e1002030.
[23] T.M. Wishart, J.P.-W. Huang, L.M. Murray, D.J. Lamont, C.A. Mutsaers, J. Ross, P. Geldsetzer, O. Ansorge, K. Talbot, S.H. Parson, T.H. Gillingwater, SMN deficiency disrupts brain development in a mouse model of severe spinal muscular atrophy, Hum. Mol. Genet. 19 (2010) 4216–4228.
[24] R. Fernandez, E. Pena, J. Navascues, I. Casafont, M. Lafarga, M.T. Berciano, cAMP-dependent reorganization of the Cajal bodies and splicing machinery in cultured Schwann cells, Glia 40 (2002) 378–388.
[25] S. Tisdale, F. Lotti, L. Saieva, J.P. Van Meerbeke, T.O. Crawford, C.J. Sumner, G.Z. Mentis, L. Pellizzoni, SMN is essential for the biogenesis of U7 small nuclear ribonucleoprotein and 3′-end formation of histone mRNAs, Cell Rep. 5 (2013) 1187–1195.
[26] M.R. Frey, A.G. Matera, Coiled bodies contain U7 small nuclear RNA and associate with specific DNA sequences in interphase human cells, Proc. Natl. Acad. Sci. U. S. A. 92 (1995) 5915–5919.
[27] S. Fayzullina, L.J. Martin, Skeletal muscle DNA damage precedes spinal motor neuron DNA damage in a mouse model of spinal muscular atrophy (SMA), PLoS One 9 (2014) e93329.
[28] M. Sabra, P. Texier, J. El Maalouf, P. Lomonte, The Tudor protein survival motor neuron (SMN) is a chromatin-binding protein that interacts with methylated lysine 79 of histone H3, J. Cell Sci. 126 (2013) 3664–3677.
[29] Y. Huyen, O. Zgheib, R.A. Ditullio Jr., V.G. Gorgoulis, P. Zacharatos, T.J. Petty, E.A. Sheston, H.S. Mellert, E.S. Stavridi, T.D. Halazonetis, Methylated lysine 79 of histone H3 targets 53BP1 to DNA double-strand breaks, Nature 432 (2004) 406–411.
[30] W.-Y. Wang, L. Pan, S.C. Su, E.J. Quinn, M. Sasaki, J.C. Jimenez, I.R.A. Mackenzie, E.J. Huang, L.-H. Tsai, Interaction of FUS and HDAC1 regulates DNA damage response and repair in neurons, Nat. Neurosci. 16 (2013) 1383–1391.
[31] E.E. Swayze, A.M. Siwkowski, E.V. Wancewicz, M.T. Migawa, T.K. Wyrzykiewicz, G. Hung, B.P. Monia, C.F. Bennett, Antisense oligonucleotides containing locked nucleic acid improve potency but cause significant hepatotoxicity in animals, Nucleic Acids Res. 35 (2007) 687–700.
[32] F. Rigo, S.J. Chun, D.A. Norris, G. Hung, S. Lee, J. Matson, R.A. Fey, H. Gaus, Y. Hua, J.S. Grundy, A.R. Krainer, S.P. Henry, C.F. Bennett, Pharmacology of a central nervous system delivered 2′-*O*-methoxyethyl-modified survival of motor neuron splicing oligonucleotide in mice and nonhuman primates, J. Pharmacol. Exp. Ther. 350 (2014) 46–55.
[33] Y. Benjamini, Y. Hochberg, Controlling the false discovery rate: a practical and powerful approach to multiple testing, J. R. Stat. Soc. Ser. B Stat. Methodol. 57 (1995) 289–300.
[34] K.J. Livak, T.D. Schmittgen, Analysis of relative gene expression data using real-time quantitative PCR and the $2^{-\Delta\Delta CT}$ method, Methods 25 (2001) 402–408.